Submillimeter-Resolution MR of the Endolymphatic Sac in Healthy Subjects and Patients with Meniere Disease

Petra Schmalbrock, Theodora Dailiana, Donald W. Chakeres, Mary C. Oehler, D. Bradley Welling, Phillipp M. Williams, and Lynette Roth

PURPOSE: To evaluate the utility of submillimeter-resolution MR imaging for direct depiction of functional soft-tissue components of the intraosseous endolymphatic duct and sac in healthy subjects and in patients with Meniere disease. **METHODS:** Axial MR images were acquired of 14 patients with Meniere disease and 14 healthy volunteers at 1.5 T with a short-echo-time steady-state 3-D gradient-echo sequence. Seven volunteers and eight patients were also studied with a T1-weighted 3-D spoiled gradient-echo sequence. T1/T2 relaxation times were estimated from studies with multiple flip angles. **RESULTS:** Independent of the acquisition method, intraosseous endolymphatic ducts and sacs were seen unambiguously in the ears of 20 of 21 healthy subjects but in only four of 12 asymptomatic and two of 10 symptomatic ears of patients with Meniere disease. Other labyrinthine structures were well depicted in all subjects. Furthermore, shorter relaxation times were measured for the contents of the vestibular aqueduct than for other labyrinthine structures. **CONCLUSION:** In our high-resolution study, the intraosseous portions of the endolymphatic ducts and sacs were depicted in most of the healthy subjects. They were frequently not seen in either ear of patients with unilateral Meniere disease, presumably because of their small size.

Index terms: Meniere disease; Temporal bone, magnetic resonance

AJNR Am J Neuroradiol 17:1707–1716, October 1996

It is most commonly assumed that the symptoms of Meniere disease are caused by endolymphatic hydrops; that is, increased endolymphatic pressure leading to an enlargement of the endolymphatic compartments in the cochlea and vestibule (1, 2). It has further been postulated that hydrops in Meniere disease may be caused by a small or malfunctioning endolymphatic sac, which also may be located abnormally (1–6).

The endolymphatic system encompasses a closed fluid compartment within the temporal bone that is continuous through the cochlea, semicircular canals, and vestibule (7). The endolymphatic system leaves the posterior vestibule at the internal aperture of the bony vestibular aqueduct and continues through the endolymphatic duct, which ends at the isthmus (1, 5, 8). From there, the endolymphatic system continues as the endolymphatic sac (1, 5, 9, 10). The intraosseous part of the endolymphatic sac, also called the *rugose* portion, is contained in the bony vestibular aqueduct and considered to be the most active component of the structure (5). The extraosseous part of the endolymphatic sac extends through the external aperture of the vestibular aqueduct into the dura of the posterior cranial fossa (1, 5, 10). The rugose portion of the endolymphatic sac is filled with epithelium-lined interconnected tubules surrounded by richly vascular fibroareolar stroma (11, 12).

In histopathologic studies of the temporal bones of patients with Meniere disease and healthy control subjects, Sando and Ikeda measured the geometric proportions of the vestibu-

Received December 14, 1995; accepted after revision April 29, 1996.

This work was supported in part by research grant 5 R29 DC 01646–03 from the National Institute on Deafness and Other Communication Disorders, National Institutes of Health.

From the Departments of Radiology (P.S., T.D., D.W.C., M.C.O., P.M.W.) and Otolaryngology (D.B.W., L.R.), Ohio State University, Columbus.

Address reprint requests to Petra Schmalbrock, PhD, Department of Radiology, MRI Facility, Ohio State University, 1630 Upham Dr, Columbus, OH 43210.

AJNR 17:1707–1716, Oct 1996 0195-6108/96/1709–1707

© American Society of Neuroradiology

lar aqueduct (3) and its contents, the endolymphatic duct and sac (4). They found that small tubelike vestibular aqueducts are more prevalent in specimens obtained from Meniere patients, whereas larger funnel-shaped vestibular aqueducts were more common in the healthy population, and that there is an association between the size of the vestibular aqueduct and that of the intraosseous portion of the endolymphatic sac (4). However, there was a distribution of shapes and sizes in both groups. More recently, Hebbar et al (6) confirmed that vestibular aqueducts and endolymphatic sacs are reduced in symptomatic ears of patients with Meniere disease compared with those of healthy control subjects and of asymptomatic contralateral ears in Meniere patients. The cause of size variations and their connection to Meniere disease remain controversial: morphologic differences may suggest a congenital predisposition for this disorder (2, 3, 13, 14). Histopathologic studies suggest perisacculus fibrosis (4, 15), altered glycoprotein metabolism (4–6), or viral infection (1, 16) as underlying pathogenic mechanisms.

Differences in the temporal bones of Meniere patients were also shown in radiographic studies (17) and more clearly with high-resolution computed tomography (CT) (18–20).Yamamoto et al found a statistically significant reduction in the size of the external aperture of the vestibular aqueduct in Meniere patients compared with that in control subjects (18, 19). Meniere disease has also been studied by magnetic resonance (MR) imaging. Tanioka et al (21) report that intraosseous endolymphatic ducts and sacs could be seen bilaterally in all healthy subjects (40 of 40 cases) and all (12 of 12) asymptomatic ears of patients with unilateral Meniere disease, whereas they were not (10 of 12) or only partially (2 of 12) seen in the symptomatic ears. Casselman et al (22, 23) report that MR imaging is useful in the evaluation of patients with symptoms similar to Meniere disease to rule out other causes, such as acoustic neuroma, schwannoma, and so on. However, no specific findings for patients with Meniere disease were reported. In a more recent article, Albers and Casselman (24) report depiction of 73% of the endolymphatic ducts and sacs in a healthy control group but narrowed or unseen endolymphatic ducts and sacs in 74% of symptomatic ears in patients with Meniere disease. Vignaud et al (25) report no abnormal findings in a study of 25 patients with Meniere disease.

On the basis of our current understanding of the causes of Meniere disease, treatment choices include low-salt diets and diuretics, and endolymphatic sac shunt surgery to reduce the endolymphatic pressure. However, this treatment is not always effective. Another, though more aggressive, choice is the destruction of vestibular function by ototoxic agents, such as streptomycin, or by vestibular nerve section. It was previously speculated that "drainage operations on patients with non-visible ducts are probably meaningless" (17). However, Leuwer et al (20) found no correlation between depiction or size of the vestibular aqueduct and the success of shunt surgery.

Unlike CT, which depicts only the bony canal of the vestibular aqueduct, MR imaging depicts the soft-tissue components directly. Thus, one might expect that MR imaging may be potentially more accurate in depicting abnormalities, such as obliteration of the duct or signal variations in the endolymphatic sac related to reduced resorption of endolymphatic fluid. The purpose of our study was to test whether we could identify any morphologic changes in Meniere patients relative to a control group of healthy subjects by using a previously developed high-resolution steady-state MR imaging technique (26–28). If abnormalities could be detected with MR imaging, this would not only be of diagnostic value but would shed further light on the pathogenesis of Meniere disease and provide helpful information for the selection of treatment choices.

Subjects and Methods

We studied 14 patients (21 to 69 years old) who had unilateral Meniere disease as determined by symptoms of fluctuating sensorineural hearing loss, tinnitus, and episodic vertigo. Audiometric testing and electronystagmography were also performed (29, 30). All patients were studied between episodes of vertigo. Onset of symptoms was reported to be more than 2 years (range, 2 to 14 years) before the MR study in all but one case (3 months). In addition, we imaged a control group of 14 healthy subjects (23 to 64 years old). Informed consent was obtained before all studies. Axial submillimeter-resolution images were acquired on a 1.5-T system using dedicated phased-array radio frequency receiver coils (31) and a prototype three-dimensional Fourier transform gradient-echo pulse sequence (27). This method uses modified phase-encode gradients to obtain very short echo times (TEs) of 3.8 milliseconds, which is of utmost importance for high-quality gradient-echo imaging of structures of the otic capsule (28). Somewhat T2-weighted steady-state images with high signal for stationary fluid in the membranous laby-

rinth were generated by using short repetition times (TRs) of 20 to 23 milliseconds, a 40° flip angle, and gradient schemes that preserve coherent transverse magnetization (26). Spatial resolution parameters included a field of view of 20 cm, section thickness of 0.7 mm, matrix size of 512 × 288 × 64, and pixel sizes of 0.35 × 0.63 × 0.7 mm^3. To assess the reproducibility of the results, three healthy subjects and five patients with Meniere disease were studied repeatedly with this steady-state sequence.

In addition, eight of the 14 Meniere patients and seven of the 14 healthy subjects were studied with a T1-weighted sequence similar to the one used by Tanioka et al (21). Images were acquired using a radio frequency–spoiled (32) fast 3-D gradient-echo sequence (3-D FSPGR) with parameters of 100/4.6 (TR/TE), 25° flip angle, 15-cm field of view, 1.0-mm section thickness, matrix size of 256 × 256 × 16, and pixel size of 0.59 × 0.59 × 1.0 mm^3. Even though the T1-weighted study used slightly larger voxel sizes, the theoretical signal-to-noise ratios (SNRs) for both acquisition methods were similar (steady-state SNR factor, 1.00; T1-weighted SNR factor, 1.06), because the steady-state data were obtained with more phase-encoding steps.

Since initial studies indicated a different signal behavior for the soft-tissue content of the vestibular aqueduct than for other membranous labyrinthine structures, additional studies of healthy subjects were obtained that permitted estimation of T1/T2 values for various structures of the otic capsule. Steady-state and radio frequency–spoiled images were acquired with slightly lower spatial resolution (field of view, 20; section thickness, 1.5 mm; matrix size, 512 × 256 × 64), TR/TE of 30/3.8, and flip angles ranging from 15° to 60°. Using the MR system's region of interest analysis tool, we measured signal intensities on these images for brain tissue in the region of the temporal lobe containing both gray and white matter, cerebrospinal fluid in the cerebellopontine angle, vestibule, cochlea, and internal auditory canal, and for the soft-tissue content of the vestibular aqueduct. To estimate T1 and T2 values, the measured signal intensities were compared with theoretical signal intensity calculations computed for different T1 and T2 values (33). First, the 3-D FSPGR data were fitted to estimate T1. Next, these T1 values were used to compute steady-state signal intensities, thus giving estimated values for T2.

Magnified axial images containing inner ear structures were displayed for all studies (steady state, ×3 magnification; T1-weighted, ×2.5 magnification). Various image contrast settings (window/level) were tested while the magnified image region containing the intraosseous endolymphatic duct and sac was observed. On images with optimized contrast, three neuroradiologists determined whether the endolymphatic sacs were either "seen" or "not seen." To be characterized as "seen," the endolymphatic sac had to be clearly visible in more than one axial section. "Not seen" meant that no signal was observed in image regions of the endolymphatic sac regardless of the contrast setting. The sections that contained the endolymphatic sac were counted. In addition, the shortest distance between the posterior semicircular canal and the subarachnoid space (posterior fossa) and the distance between the most posterior portion of the vestibule (at the junction with the common crus) and the subarachnoid space were measured.

Additional confirmation for the depiction of intraosseous endolymphatic sacs was obtained by image postprocessing. The fastest way to produce a single image of the endolymphatic sac was with oblique coronal reformatted images depicting the endolymphatic sac as a triangular structure (34). In addition, restricted maximum intensity projection and 3-D volume-rendered images were generated using the postprocessing tools on a workstation (General Electric [Milwaukee, Wis] Advantage Windows Station).

Results

With the steady-state sequence, high-quality images (Figs 1–3A) depicting small temporal bone anatomic structures were obtained in most studies (12 of 14 patients with Meniere disease and 11 of 14 healthy subjects). Visible structures included the internal auditory canal, the vestibulocochlear and facial nerves, the vestibule, the cochlea, and the semicircular canals. In many cases, the spiral osseous lamina in the cochlea could be identified. The cerebrospinal fluid signal in the cerebellopontine angle was reduced because of fluid motion. On the T1-weighted images, the membranous labyrinthine fluid had lower signal intensity, thus impairing the depiction of some structures (Figs 1–3B). Since spatial resolution was high in all three dimensions, high-quality reformatted images could be generated in orthogonal (Figs 1–3) and oblique (Fig 1E and F) reformatted planes or in surface reconstructions (Fig 4). The latter were found helpful in determining the 3-D relationships among the structures.

Visibility of the intraosseous endolymphatic duct and sac varied even though uniformly high image quality was obtained for all other anatomic structures. Although the sacs were clearly seen for most healthy subjects (Fig 1) and for some Meniere patients (Fig 2) with both the steady-state and the T1-weighted sequences, in other cases, they could not be seen (Fig 3). Summaries of the visibility of the endolymphatic sac in the ears of healthy subjects and in the symptomatic and asymptomatic ears of Meniere patients are given in Tables 1 and 2, respectively. Repeated studies gave identical results in all cases in which such data were acquired. In all but one healthy subject, the

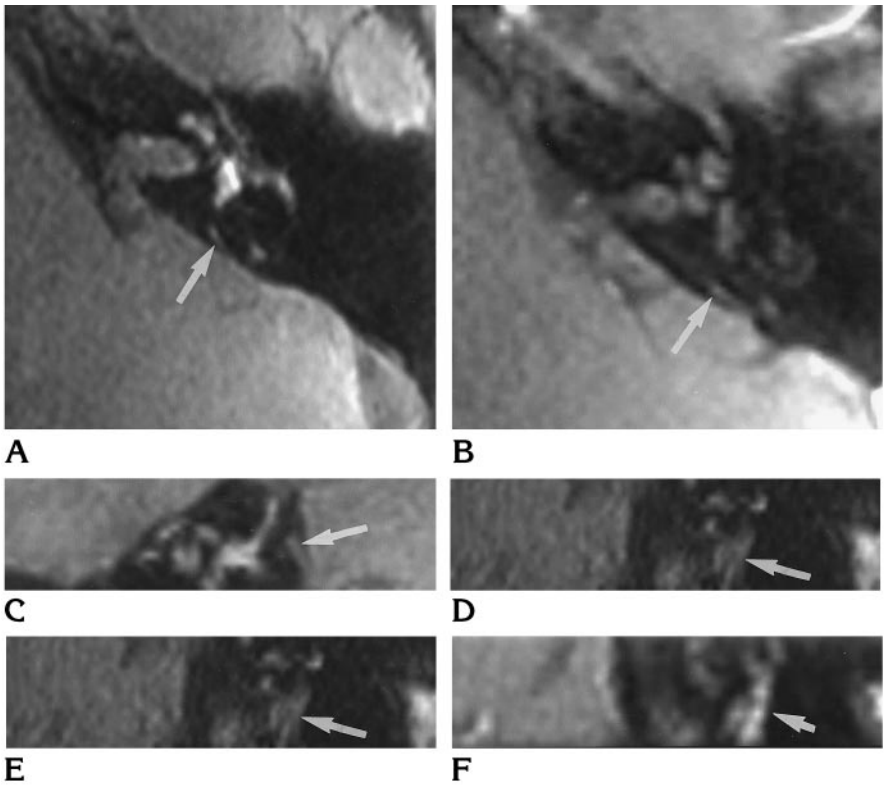

Fig 1. Steady-state (*A, C, E*) and T1-weighted (*B, D, F*) MR images in a healthy 25-year-old woman (subject 6 in Table 1).

The endolymphatic sac (*arrows*) is depicted on axial (*A* and *B*), reformatted sagittal (*C* and *D*), and oblique coronal (*E* and *F*) images. Note that the portions of the membranous labyrinth that are filled with stationary fluid, including the internal auditory canal, vestibule, cochlea, and semicircular canals, are better delineated on the steady-state images than on the T1-weighted images. Moving fluid in the cerebellopontine angle has low signal on both sequences. The intraosseous portion of the endolymphatic sac has fairly high signal on both sequences, indicating different tissue characteristics than other portions of the membranous labyrinth.

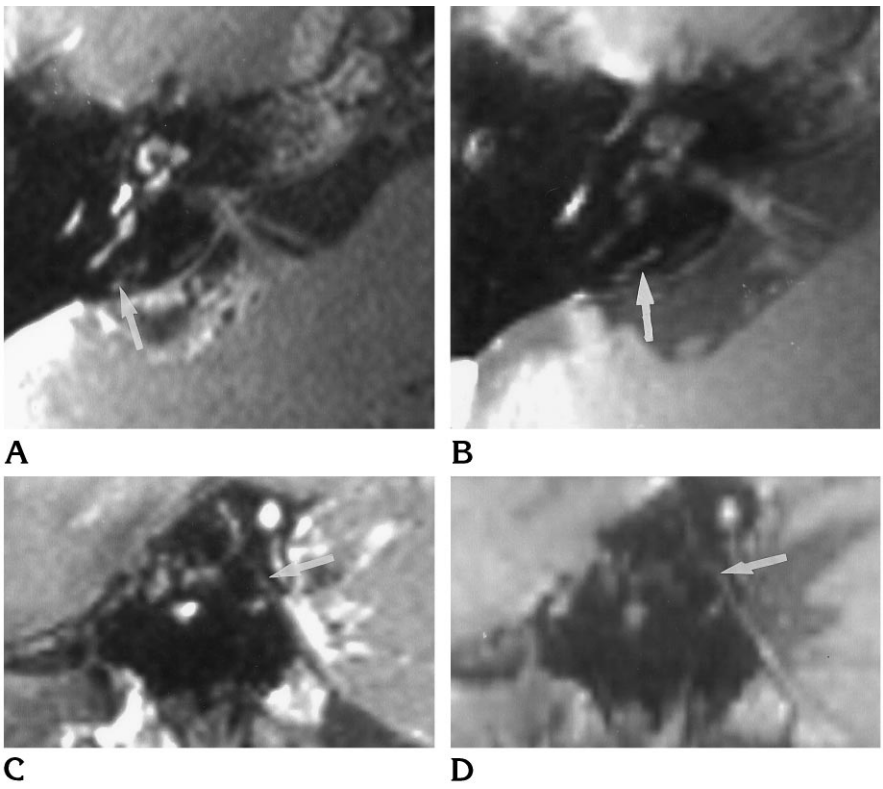

Fig 2. Steady state (*A* and *C*) and T1-weighted (*B* and *D*) MR images of the symptomatic ear of a 65-year old woman with a 4-year history of Meniere disease (subject 6 in Table 2).

The endolymphatic sac (*arrows*) can be clearly seen on the axial (*A* and *B*) and sagittal (*C* and *D*) images.

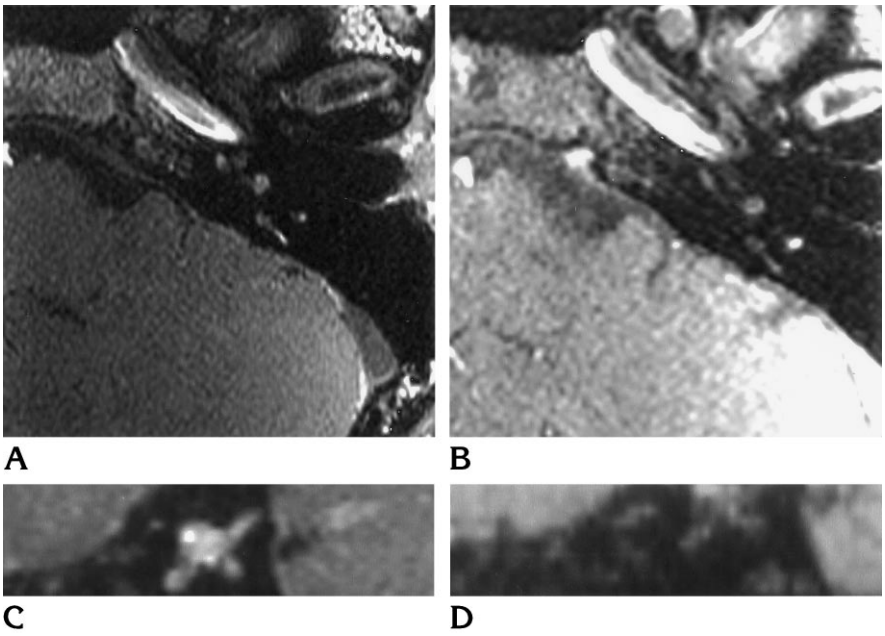

Fig 3. Steady state (*A* and *C*) and T1-weighted (*B* and *D*) MR images of the symptomatic ear of a 50-year-old man with a 5-year history of Meniere disease in whom the sacs were not depicted (subject 8 in Table 2). Even though the other inner ear structures are clearly depicted on the axial (*A* and *B*) and sagittal (*C* and *D*) images, the endolymphatic sac is not seen in this case.

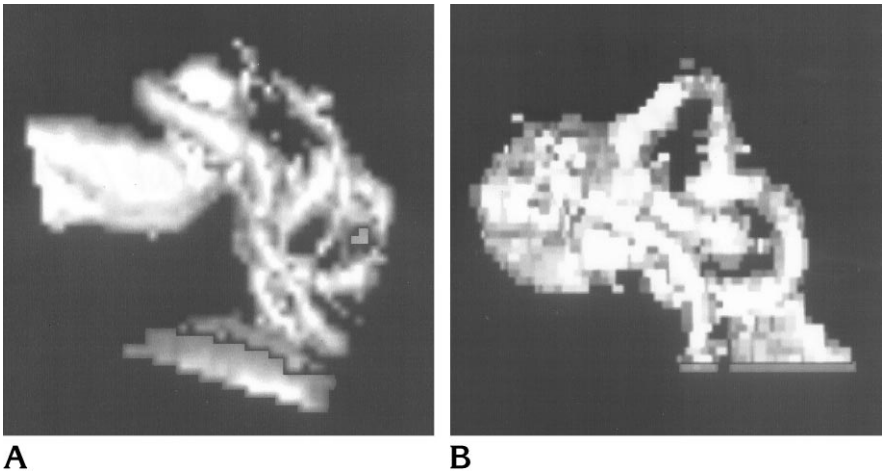

Fig 4. Surface-rendered images depict craniocaudal (*A*) and anteroposterior (*B*) views of the membranous labyrinth in a healthy volunteer.

findings between the steady-state and T1-weighted sequences agreed. Including only inner ears with consistent findings, intraosseous endolymphatic sacs were seen in 20 (95%) of 21 ears in healthy subjects and in four (33%) of 12 asymptomatic and two (20%) of 10 symptomatic ears in Meniere patients. For the two Meniere patients who were examined after surgery, only the data for the contralateral asymptomatic ear are included in this summary. In two patients with unilateral Meniere disease, sacs were seen bilaterally; and in two other cases, an endolymphatic sac was seen only on the asymptomatic side.

Although visibility or lack of visibility of the endolymphatic sacs was not affected by the choice of pulse sequence, the T1-weighted images often depicted the sacs with slightly higher quality (Figs 1 and 2). Measurements of T1/T2 resulted in lower values, 850/100, for the contents of the vestibular aqueduct as compared with 2000/1000 (26) for other structures of the membranous labyrinth (Fig 5). For the acquisition parameters used in our study, these T1/T2 values theoretically lead to a 1.8-fold signal decrease for the tissue content in the vestibular aqueduct in steady state as compared with T1-weighted images (steady-state signal of the contents of the vestibular aqueduct, 0.14; T1-weighted signal, 0.24). For the other fluid-filled

TABLE 1: Visibility of the endolymphatic sac in healthy subjects

Subject	Age, y/Sex	Steady State		T1-Weighted	
		R	L	R	L
1	23/M	+	−	+	+
2	64/F	+	+	+	+
3	64/M	†	†	‡	+
4	47/M	+	−	+	−
5*	40/F	+	+	+	‡
6	25/F	+	+	+	+
7	26/M	+	+	...	...
8*	24/M	+	+	...	...
9*	44/M	+	+	...	...
10	51/F	+	+	...	...
11	59/F	+	+	...	...
12	30/F	+	+	...	...

Note.—+ indicates the endolymphatic sac was seen; − indicates not seen.

* Subject was studied twice.

† Study was of poor quality.

‡ Not included in image region.

TABLE 2: Visibility of the endolymphatic sac in patients with Meniere disease

Patient	Age, y/Sex	Symptomatic Side	Steady State		T1-Weighted	
			R	L	R	L
1*	60/F	R	†	−	†	−
2*	63/F	R	−	−	−	−
3	18/M	R	−	−	...	...
4	39/F	R	−	+	...	...
5	64/F	R	+	+	+	‡
6	65/F	R	+	+	+	+
7*	44/F	L	+	−	+	−
8*	50/M	L	−	−	−	−
9*	57/M	L	−	−	−	−
10	42/F	L	−	−	...	...
11	44/F	L	−	−	...	...
12	53/F	L	−	†	−	†

Note.—+ indicates the endolymphatic sac was seen; − indicates not seen.

* Patient was studied twice.

† Patient was studied after surgery.

‡ Not included in image region.

labyrinthine structures, a 1.6-fold signal increase is expected with the steady-state sequence (steady-state signal of fluid, 0.24; T1-weighted signal, 0.15).

The results for the distance measurements between the posterior semicircular canal and the subarachnoid space and between the vestibule and the subarachnoid space are depicted in Figure 6. The thickness of the temporal bone in these locations was larger in healthy subjects with visible endolymphatic sacs (vestibule–subarachnoid, 6.8 ± 2.5; posterior semicircular ca-

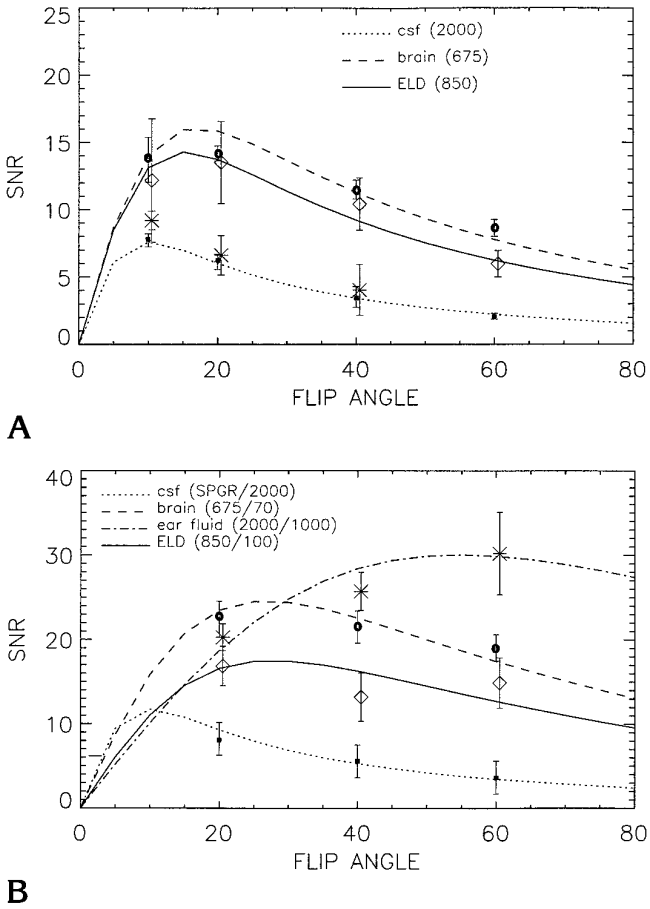

Fig 5. Experimental and theoretical signal intensities as a function of the flip angle in 3-D FSPGR (*A*) and steady-state (*B*) images. Calculated signal intensities (*lines*) were compared with measured signal intensities (*symbols with error bars*) for brain tissue in the temporal lobe (*circles*), cerebrospinal fluid in the cerebellopontine angle (*squares*), vestibule, internal auditory canal, and cochlea (*asterisks*), and in the contents of the vestibular aqueduct (*diamonds*).

In *A*, the signal for cerebrospinal fluid and inner ear fluid matched computations (*dotted line*) for a T1 of 2000, and the brain signal from a region containing both gray and white matter matched a T1 of 675 (*dashed line*). The signal for the contents of the vestibular aqueduct was markedly different from the signal for fluid and brain, and best matched computations for a T1 of 850 (*solid line*).

In *B*, the signal characteristic for moving cerebrospinal fluid in the cerebellopontine angle is identical to the signal characteristic in the 3-D FSPGR data, because motion leads to loss of coherent transverse magnetization and reduced signal. The stationary inner ear fluid yields higher signal and matches computations for T1/T2 of 2000/1000 (*dashed-dotted line*). Brain signal matches T1/T2 of 675/70. Again, the signal for the contents of the vestibular aqueduct is different from that for other tissues. Computations of T1/T2 = 850/100 best fit the data.

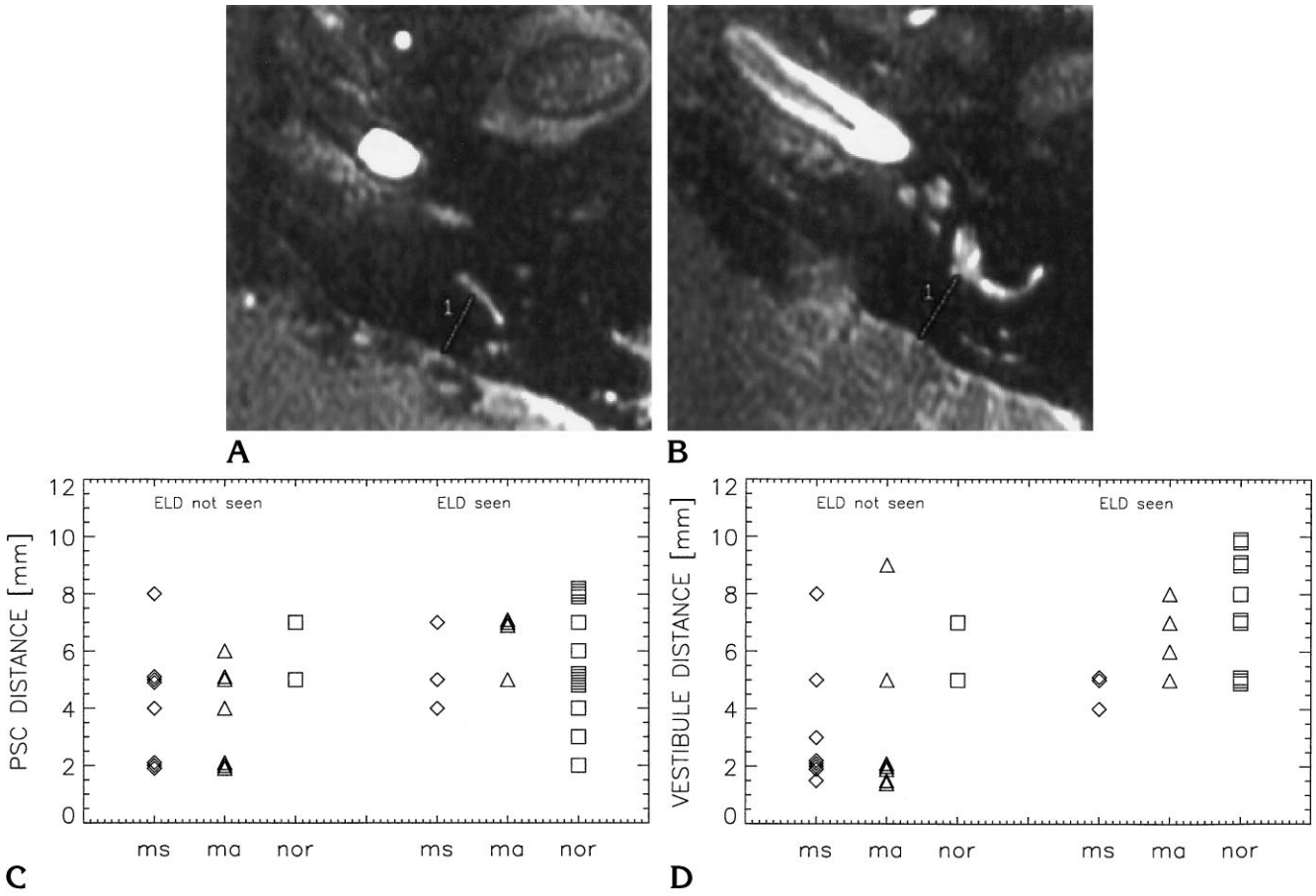

Fig 6. Measurements of temporal bone dimensions.

A and *B*, Axial images indicate positions for distance measurements between the vestibule and the subarachnoid space and between the posterior semicircular canal and the subarachnoid space.

C and *D*, Corresponding distribution of distances among depicted and nondepicted endolymphatic sacs for normal (*nor, diamonds*) ears and symptomatic (*ms, triangles*) and asymptomatic (*ma, squares*) ears in Meniere patients.

nal–subarachnoid, 5.8 ± 2.2) than it was in the symptomatic and asymptomatic ears of Meniere patients with nondepicted endolymphatic sacs (vestibule–subarachnoid, 3.2 ± 2.2 for symptomatic ears; 3.1 ± 2.9 for asymptomatic ears; posterior semicircular canal–subarachnoid, 4.1 ± 2.1 for symptomatic ears; 3.2 ± 1.7 for asymptomatic ears). Larger distances were measured in Meniere patients with visible endolymphatic sacs (vestibule–subarachnoid, 4.7 ± 0.6 for symptomatic ears; 6.5 ± 1.3 for asymptomatic ears; posterior semicircular canal–subarachnoid, 5.3 ± 1.5 for symptomatic ears; 6.5 ± 1.0 for asymptomatic ears).

Discussion

Our work indicates that intraosseous endolymphatic ducts and sacs are more frequently seen in the healthy population than in either ear of patients with unilateral Meniere disease. Furthermore, the nondepiction of sacs seems to correlate with a smaller temporal bone width between the posterior semicircular canal/vestibule and the subarachnoid space.

Our findings are different from those of previous MR imaging studies. Unlike Tanioka et al (21), who report nondepiction of the sacs only in symptomatic Meniere ears, we found nondepiction bilaterally in a majority of cases. Since we obtained this finding both with our steady-state sequence and with a T1-weighted sequences similar to the one used by Tanioka et al, the reasons for these discrepancies are unclear. Albers and Casselman (24) reported fewer visible endolymphatic sacs (73%) than found in our study (95%). Lower spatial resolution and use of a different pulse sequence (constructive interference in steady state, or CISS) may explain this difference. Furthermore, nar-

rowed or unseen endolymphatic ducts and sacs occurred in 74% of symptomatic ears in patients with Meniere disease in the study by Albers and Casselman as compared with similar findings of 80% in our study. In distinction to the MR imaging studies, Leuwer et al report 100% visibility of vestibular aqueducts with ultra-high-resolution CT (20).

Several possible causes could account for the nondepiction of endolymphatic ducts and sacs in our MR imaging study. Early on, we suspected altered fluid motion to be the cause of signal loss in the steady-state images, since even very small amounts of motion can destroy coherent transverse magnetization, leading to reduced signal (33). However, endolymphatic sacs were also not seen on the T1-weighted images, which are insensitive to this phenomenon. Furthermore, unlike other portions of the membranous labyrinth, the rugose portion of the endolymphatic sac is filled with epithelial-lined interconnected tubules surrounded by richly vascular fibroareolar stroma (11, 12), and one might expect stagnant fluid. For these reasons, altered fluid motion appears to be an unlikely hypothesis for the nondepiction of endolymphatic sacs.

A second hypothesis for the nondepiction of the sacs may be that variations in tissue composition of the contents of the vestibular aqueduct alter the T1 and T2 relaxation times. Our T1/T2 measurement of the contents of the vestibular aqueduct in healthy subjects suggests that the tissue-filled rugose portion of the endolymphatic sac indeed leads to reduced T1/T2 relaxation times compared with other fluid-filled structures of the inner ear. It may thus be reasonable to assume that an increase of nonfluid tissue components in the sac or altered tissue density may lead to decreased signal, thus preventing depiction of the endolymphatic sac. Increased spatial resolution and acquisition parameters that are more sensitive to nonfluid signal are needed to further evaluate this hypothesis.

Finally, the nondepiction of the endolymphatic duct and sac may simply be due to their reported small size in patients with Meniere disease. For example, Sando and Ikeda (3) give sizes of 0.3 to 0.5 mm for tubelike vestibular aqueducts with corresponding sizes for the intraosseous endolymphatic sac (4). With voxel sizes of $0.35 \times 0.63 \times 0.7$ mm^3 to $0.59 \times 0.59 \times 1.0$ mm^3 used in this study, this size is just at the resolution limit. This seems to indicate that small sacs, which are more prevalent in Meniere patients, cannot be resolved with the resolution capabilities of our study.

Higher SNRs are needed to improve further the spatial resolution for inner ear studies. This may be achieved by further improvements in radio frequency coil design (35) or in image postprocessing (36). Computer simulations were carried out to assess how pulse sequence parameters can be further optimized for improved SNR in the vestibular aqueduct contents and other structures of the membranous labyrinth. Signal intensities were computed for different TRs and flip angles and for spoiled gradient-echo and steady-state sequences using the measured T1/T2 values (850/100 for the vestibular aqueduct contents and 2000/1000 for fluid). For the 3-D FSPGR sequence, no SNR improvement can be achieved within reasonable scan times. However, our computations indicate that similar SNR can be achieved in the same scan time with a TR of 50, a flip angle of 15° to 20°, and 32 sections, and with a TR of 100, a flip angle of 25°, and 16 sections. Since we found correct positioning of the narrow acquisition slab (16 sections $\times$ 1 mm) difficult, it would be advantageous to acquire more sections with a shorter TR. With the steady-state sequence, the signal intensity is nearly independent of TR. This suggests that SNR can be improved by using a shorter TR and more signal averages or sections. However, a shorter TR will require faster and stronger gradient hardware. The computations also indicate that a small signal increase may be achieved for the vestibular aqueduct with a lower flip angle (30° instead of 40° in our study). Similar arguments may be made for improving SNR and contrast in CISS sequences. Thin-section fast spin-echo imaging is another technique that generates excellent depiction of the membranous labyrinth (37). We included fast spin-echo imaging in some of our studies; however, the intraosseous endolymphatic duct and sac were generally not seen. Perhaps the minimal section thickness of 3 mm available to us at the time was too large and the shorter T2 relaxation time for the vestibular aqueduct contents led to lower signal on T2-weighted fast spin-echo images.

An additional difficulty with identifying small endolymphatic sacs may be overcome by postprocessing techniques. These small structures appear only in a few pixels distributed over

three to eight sections, making them difficult to differentiate from background noise. A postprocessing technique, such as a restricted maximum intensity projection for a designated 3-D region that contains the vestibular aqueduct, may join pixels from individual images and form a more easily discernible line in the processed image.

Even though further technical improvements are needed for MR imaging studies in Meniere disease, it may be possible to draw some preliminary conclusions regarding the potential usefulness of MR imaging in the evaluation of this disorder. Our study may lend additional support to the hypothesis that there is a congenital predisposition for Meniere disease (2, 19), because (*a*) morphologic variations were found bilaterally in Meniere patients with unilateral disease and (*b*) nondepicted, presumably small, sacs were associated with a narrow temporal bone between the vestibule and posterior semicircular canal and the subarachnoid space. Given the noninvasive nature of MR imaging, it may be useful as a tool for investigating the hereditary aspects of Meniere disease. Furthermore, MR imaging may be valuable for presurgical evaluation before shunt surgery. However, in our preliminary study, only three of the 14 patients had surgery after the MR study. In two of these cases, sacs were not seen and shunting led to insignificant or limited control of vertigo. In the third case, sacs were seen bilaterally, but shunt surgery was performed only recently and it is too early to judge the success of the surgical procedure by rigid criteria (30). Since our preliminary result is not yet statistically significant, further tests are needed to assess whether visibility of the intraosseous endolymphatic duct and sac on MR images may be indicative of the success of surgical shunting procedures.

References

1. Wackym PA. Histopathological findings in Meniere's disease. *Otolaryngol Head Neck Surg* 1995;112:90–100
2. Shea JJ. Classification of Meniere's disease. *Am J Otol* 1993;14: 224–229
3. Sando I, Ikeda M. The vestibular aqueduct in patients with Meniere's disease: a temporal bone histopathological investigation. *Acta Otolaryngol* 1984;97:558–570
4. Ikeda M, Sando I. Endolymphatic duct and sac in patients with Meniere's disease. *Ann Otol Rhinol Laryngol* 1984;93:540–546
5. Wackym PA, Linthicum FH, Ward PH, House WF, Micevych PE, Bagger-Sjö bä ck D. Re-evaluation of the role of the human endolymphatic sac in Meniere's disease. *Otolaryngol Head Neck Surg* 1990;102:732–744
6. Hebbar GK, Rask-Andersen H, Linthicum FH. Three-dimensional analysis of 61 human endolymphatic ducts and sacs in ears with and without Meniere's disease. *Ann Otol Rhinol Laryngol* 1991; 100:219–225
7. Schuknecht HF. *Pathology of the Inner Ear.* Philadelphia, Pa: Lea & Febinger; 1993:45–64
8. Friberg U, Rask-Andersen H, Bagger-Sjö bä ck D. Human endolymphatic duct. *Arch Otolaryngol* 1984;110:412–428
9. Danckwardt-Lillienströ m N, Rask-Andersen H, Linthicum FH, House WF. A technique to obtain and process surgical specimens of the human vestibular aqueduct for histopathological studies of the endolymphatic duct and sac. *ORL J Otorhinolaryngol Relat Spec* 1992;54:215–219
10. Friberg U, Jansson B, Rask-Andersen H, Bagger-Sjö bä ck D. Variations in the surgical anatomy of the endolymphatic sac. *Arch Otolaryngol Head Neck Surg* 1988;114:389–394
11. Linthicum FH, Galey FR. Computer-aided reconstruction of the endolymphatic sac. *Acta Otolaryngol* 1981;91:423–429
12. Anson BJ, Donaldson JA. *Surgical Anatomy of the Temporal Bone.* 3rd ed. Philadelphia, Pa: Saunders; 1981:480–489
13. Khtarpal U, Schuknecht HF. Temporal bone findings in a case of Meniere's disease treated by parenteral streptomycin and endolymphatic shunt. *Laryngoscope* 1990;100:407–414
14. Antunez J-CM, Linthicum FH, Galey FR, McCann GD. Computer-aided and graphic reconstruction of the human endolymphatic duct and sac: a method for comparing Meniere's and non-Meniere's disease. *Ann Otol Rhinol Laryngol* 1980;89(suppl 76):23–32
15. Arenberg IK, Norback DH, Shambaugh GE. Distribution and density of subepithelial collagen in the endolymphatic sac in patients with Meniere's disease. *Am J Otol* 1985;6:449–454
16. Welling DB, Daniels RL, Brainard J, Western LM, Prior TW. Detection of viral DNA in endolymphatic sac tissue from Meniere's disease patients. *Am J Otol* 1994;15:639–643
17. Stahle J, Wilbrand H. The vestibular aqueduct in patients with Meniere's disease: a tomographic and clinical investigation. *Acta Otolaryngol* 1974;78:36–48
18. Yamamoto E, Mizukami C. Development of the vestibular aqueduct in Meniere's disease. *Acta Otolaryngol* 1993;504(suppl): 46–50
19. Yamamoto E, Mizukami C, Isono M, Ohmurra M, Hirono Y. Observation of the external aperture of the vestibular aqueduct using three-dimensional surface reconstruction imaging. *Laryngoscope* 1991;101:480–483
20. Leuwer R, Westhofen M, Siepman G. Significance of ultra HR-CT in the preoperative diagnosis of Meniere's. *Laryngorhinootologie* 1993;71:217–220
21. Tanioka H, Zusho H, Machida T, Sasaki Y, Shirakawa T. High resolution MRI of the inner ear: findings in Meniere's disease. *Eur J Radiol* 1992;15:83–88
22. Casselman JW, Kuhweide R, Deimling M, Ampe W, Dehaene I, Meeus L. Constructive interference in steady-state-3DFT MR imaging of the inner ear and cerebellopontine angle. *AJNR Am J Neuroradiol* 1993;14:47–57
23. Casselman JW, Kuhweide R, Dehaene I, Ampe W, Devlies F. Magnetic resonance examination of the inner ear and cerebellopontine angle in patients with vertigo and/or abnormal findings at vestibular. *Acta Otolaryngol Suppl (Stockh)* 1994;513:15–27
24. Albers FWJ, Casselman JW. 3DFT-magnetic resonance imaging of the inner ear in Meniere's disease. In: Filipo R, Barbara M, eds. *Meniere's Disease: Perspectives in the 90's.* Amsterdam, Netherlands: Kugler Publications; 1994:43–46
25. Vignaud J, Marsot-Dupuch K, Pharaboz C, Derosier C, Cordoliani YS. Imaging of the vestibule. *Otolaryngol Head Neck Surg* 1995; 112:36–49

26. Schmalbrock P, Brogan MA, Chakeres DW, Hacker VA, Ying K, Clymer BD. Contrast optimization for submillimeter resolution imaging of the inner ear. *J Magn Reson Imaging* 1993;3:451–459
27. Ying K, Schmalbrock P, Clymer BD. Echo-time reduction for submillimeter resolution imaging with a phase encode time reduced acquisition method *Magn Reson Med* 1995;33:82–87
28. Oehler M, Schmalbrock P, Chakeres DW. Artifacts related to magnetic susceptibility differences between bone and air on high resolution MRI of the temporal bone. *AJNR Am J Neuroradiol* 1995;16:1135–1143
29. Barber HO, Stockwell CW. *Manual of Electronystagmography*. 2nd ed. St Louis, Mo: Mosby; 1980:191
30. Monsell EM, Committee on Hearing and Equilibrium. Guidelines for the diagnosis and evaluation of therapy in Meniere's disease. *Otolaryngol Head Neck Surg* 1985;113:181–185
31. Schmalbrock P, Pruski J, Sun L, Rao A, Monroe JW. Phased array RF coils for high-resolution imaging of the inner ear and the brain stem. *J Comput Assist Tomogr* 1995;19:8–14
32. Wehrli FW. Fast-scan magnetic resonance: principles and applications. *Magn Reson Q* 1990;6:165–236
33. van der Meulen P, Groen JP, Tinus AMC, Bruntink G. Fast field echo imaging: an overview and contrast calculations. *Magn Reson Imaging* 1988;6:355–368
34. Oehler MC, Chakeres DW, Schmalbrock P. Reformatted planar "Christmas tree": magnetic resonance imaging appearance of the endolymphatic sac. *AJNR Am J Neuroradiol 1995;16:1525–1528*
35. Wald LL, Moyer SE, Day MR, Nelson SJ, Vigneron DB. Proton spectroscopic imaging of the human brain using phased array detectors. *Magn Reson Med* 1995;34:440–445
36. Ying K, Clymer BD, Schmalbrock P. Adaptive filtering processing for magnetic resonance images. *J Magn Reson Imaging* 1996;6:367–377
37. Harnsberger HR, Dahlen RT, Shelton C, Gray SD, Parkin JL. Advanced techniques in MRI in the evaluation of the large endolymphatic duct and sac syndrome. *Laryngoscope* 1995;105:1037–1042